STUDYING TRENDS IN AEROSOL PRESENCE USING THE ABSORBING AEROSOL INDEX DERIVED FROM GOME-1, SCIAMACHY, AND GOME-2

Lieuwe G. Tilstra, Martin de Graaf, Olaf N.E. Tuinder, Ronald J. van der A, and Piet Stammes

Royal Netherlands Meteorological Institute (KNMI), Wilhelminalaan 10, De Bilt, The Netherlands

Abstract

In this paper we study 16-year long time series of the Absorbing Aerosol Index (AAI) for a selection of the most prominent aerosol producing regions on the globe. The time series of the AAI were recorded by the satellite instruments GOME-1, SCIAMACHY, and GOME-2 aboard the ERS-2, Envisat, and MetOp-A satellites, respectively. These three satellite instruments suffer, each in their own way, from severe instrument degradation in the ultraviolet (UV) wavelength range from which the AAI is derived. To be able to perform a reliable analysis on the AAI time series, we first remove the effects of instrument degradation from the Earth reflectances before calculating the AAI from them. To study the resulting time series, we use tropospheric NO_2 data as a reference in the regions dominated by biomass burning events. It is found that the regional AAI data follow the regional tropospheric NO_2 data well. Therefore, it is possible to accurately remove the effects of instrument degradation and to combine the AAI data from the three satellite instruments. The time series of the AAI for the studied aerosol regions show no clear trend over the studied 16-year time period from 1995 to 2011.

ABSORBING AEROSOL INDEX

The Absorbing Aerosol Index (AAI) is an index based on a comparison of measured UV reflectances with simulated Rayleigh reflectances. These simulated reflectances are calculated for cloud-free and aerosol-free atmospheres in which only Rayleigh scattering, absorption by molecules, Lambertian surface reflection as well as surface absorption can take place. The AAI is derived from another quantity, called the residue, which is defined as

$$r = -100 \cdot^{10} \log\left(\frac{R_\lambda^{obs}}{R_\lambda^{Ray}}\right) \tag{1}$$

In this equation, R^{obs} refers to reflectances measured by, in this case, GOME-2, while R^{Ray} refers to modelled Rayleigh reflectances. The symbol λ refers to the first, shortest wavelength of the AAI wavelength pair, which is 340 nm. The surface albedo A_s used in the simulations for this wavelength is assumed to be the same as the surface albedo at the second wavelength λ_0 = 380 nm. The surface albedo at 380 nm on its turn is found from requiring that the simulated Rayleigh reflectance equals the measured reflectance at this wavelength. That is, we have the following two constraints:

$$R_{\lambda_0}^{obs} = R_{\lambda_0}^{Ray}(A_s) \quad ; \quad A_s(\lambda) = A_s(\lambda_0) \tag{2}$$

The two equations above basically define the algorithm that is used to calculate the residue. When a positive residue is found, absorbing aerosols were detected. Negative or zero residues on the other hand suggest an absence of absorbing aerosols. Therefore, the AAI is defined as equal to the residue where the residue is positive, and it is simply not defined for negative values of the residue.

The GOME-1, SCIAMACHY, and GOME-2 AAI are developed and produced at the KNMI and the data are available for download on the TEMIS website (http://www.temis.nl/). The GOME-1 AAI data were

derived from level-1 version 4.00. The SCIAMACHY AAI data were derived from level-1 version 6.03. Since November 2009 the GOME-2 AAI is an operational product in the O3M SAF. The GOME-2 level-1b data used for this paper were generated by PPF 4.0 and above. To be more specific, reprocessed level-1b data is used from 5 January 2007 to 26 June 2008 (these are data from the so-called 'R01 reprocessing'), and for the period after this date the data were taken from the regular NRT flow of level-1b PDU data products that were disseminated by EUMETSAT via EUMETCast. For the main characteristics of the AAI products, please consult Table 1.

	AAI Wavelength pair (nm)	Equator passing time (local time)	Pixel size (km^2)	Days needed for global coverage	Platform / Satellite	Time period covered
GOME-1	340 / 380	10:30 a.m.	320 x 40	3	ERS-2	1995 – 2003
SCIAMACHY	340 / 380	10:00 a.m.	60 x 30	6	Envisat	2002 – present
GOME-2	340 / 380	09:30 a.m.	80 x 40	1.5	MetOp-A	2007 – present

Table 1: **Main characteristics of GOME-1, SCIAMACHY, and GOME-2, of their derived AAI products, and of the time periods covered by the three AAI datasets. The AAI wavelength pair is 340/380 nm in all cases.**

INSTRUMENT DEGRADATION

Instrument degradation has been shown to have a large impact on the AAI (Tilstra et al., 2010). In the current paper we will be presenting and analysing AAI data that were corrected for instrument degradation in the manner described in the paper by Tilstra et al. (2011). In this paper, the Earth reflectance measured by SCIAMACHY is corrected for the effects of instrument degradation by analysing time series of the global mean reflectance, extracting a polynomial function that describes the effects of instrument degradation, and performing the resulting correction. In this approach, the time series of the global mean reflectance are fitted with a Fourier series multiplied with a polynomial base. The Fourier terms are meant to describe the seasonal variation of the global mean reflectance. These seasonal variations are not caused by instrument degradation, and therefore disregarded. The polynomial terms, on the other hand, represent the drop in signal due to instrument degradation. Knowledge of the polynomial base allows a straightforward correction of the reflectances. The method described here was applied individually to GOME-1, SCIAMACHY, and GOME-2.

STUDYING TIME SERIES OF THE AAI

In this section we will analyse time series of the AAI from GOME-1, SCIAMACHY, and GOME-2 for a selection of known aerosol regions. The box-shaped regions are defined graphically in Figure 1.

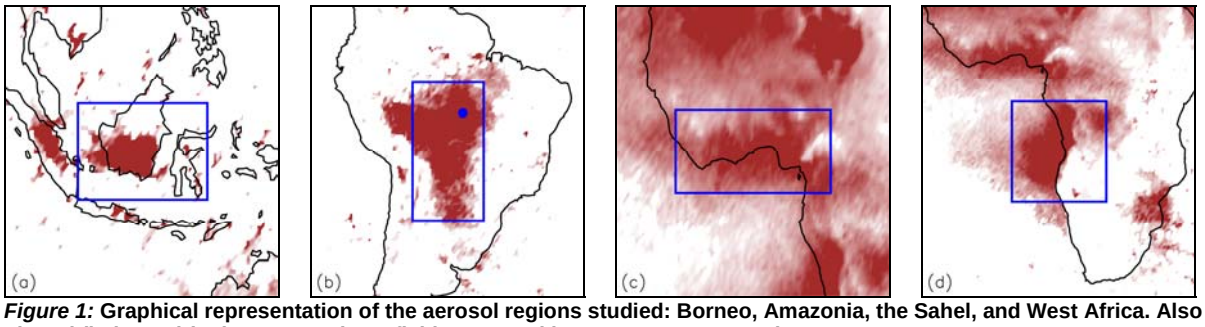

Figure 1: **Graphical representation of the aerosol regions studied: Borneo, Amazonia, the Sahel, and West Africa. Also plotted (in brown) is the averaged AAI field measured by SCIAMACHY over the years 2002–2010.**

Case A: Borneo

In Figure 2 we present the time series of the AAI for the region containing the island of Borneo as illustrated in Figure 1a. On the vertical axis we plotted the regional mean AAI, averaged with a running mean of 31 days. The red data points were measured by GOME-1, the brown data points by

SCIAMACHY, and the blue data points by GOME-2. Notice the two strong peaks in the time period 1997/1998. These were caused by forest fires due to extreme droughts in this El Niño episode. On Borneo, a total area of 120.000 km^2 forest was destroyed (Wooster and Strub, 2002).

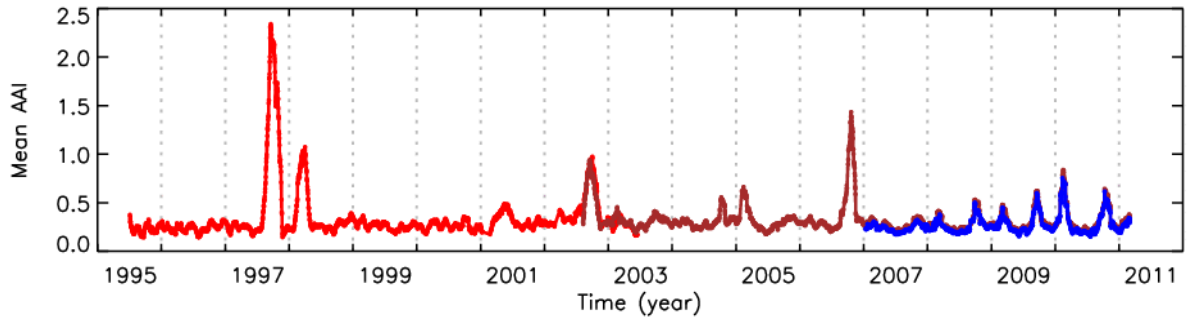

Figure 2: **Regional mean AAI for the box containing the island Borneo as a function of time over the period 1995–2011.**

From Figure 2 it is found that peaks occur once or twice a year: either in the months March/April or in the months September/October. The probability that such a peak occurs turns out to be higher in the more recent years. In a recent paper by Van der Werf et al. (2009), time series of fire emission estimates are given for a somewhat similar region as the one indicated in Figure 1a. The agreement between the time series of fire emissions given there and the AAI shown in Figure 2 is quite good.

The baseline (background level) of the AAI time series, consisting of low values of ~0.2, is stable. This is a good indication that instrument degradation was removed successfully. Also notice that the three data sets overlap consistently with each other where they overlap in time.

Case B: Amazonia

The mean AAI for the Amazonia region is presented in Figure 3. There is a strong seasonal cycle, and a strong year-to-year variation. In most years, there is a strong biomass burning peak present in the months August/September. For a qualitative validation we can again make use of results from the paper by Van der Werf et al. (2009). The agreement is again quite satisfactory. To get to a more quantitative validation, we resort to AERONET data of station “Alta Floresta”. This station is represented by the blue dot in Figure 1b. We used level 2.0 data, and only accepted measurements which had a measurement time close to the local measurement time of GOME-1, SCIAMACHY, and GOME-2. Furthermore, we applied a running mean of 11 days. The result is shown in Figure 4.

From a qualitative point of view there is certainly agreement, but there is also quite a poor correlation between the peak heights found in Figure 3 and those found in Figure 4. Efforts to improve the correlation by reducing the size of the box shown in Figure 1b, in order to make it agree more with the observational area of the AERONET station, were only partly successful. Possible explanations for the remaining differences are the cloud screening in the AERONET level 2.0 data and the fact that the AAI and AOT are by definition not related by a fixed unique relationship. Also the large amount of missing AERONET data might play a role in the discrepancies found.

In a next attempt to validate the AAI time series we analyse tropospheric NO_2 data measured by the instruments GOME-1 and SCIAMACHY for the same region and for the same time period. Emission of NO_2 by biomass burning processes is well-known (e.g. Van der A et al., 2006, 2008). Since the area studied is a typical biomass burning region, we would expect some sort of correlation between the concentration of aerosols and that of the tropospheric NO_2 column (cf. Veefkind et al., 2011). In Figure 5 we present the tropospheric NO_2 column, measured by GOME-1 and SCIAMACHY, averaged over the studied region and treated with a running mean of 31 days. The GOME-1 data are plotted using the light blue colour and the dark blue colour is used to denote the SCIAMACHY data.

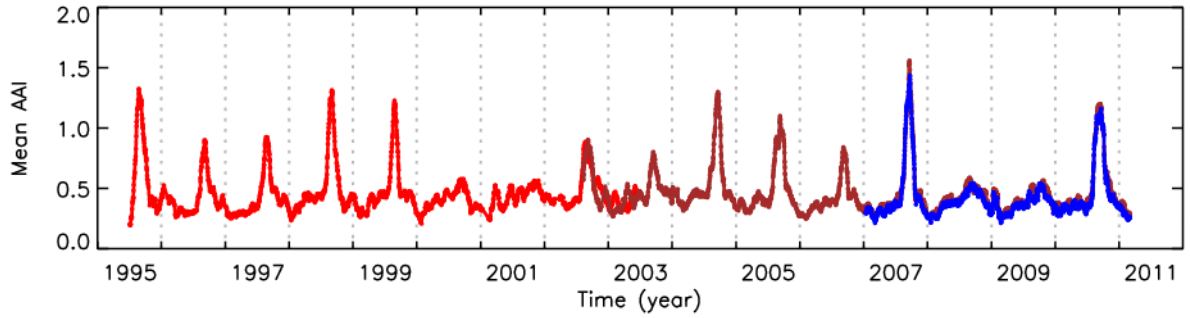

Figure 3: **Mean AAI for the Amazonian box as a function of time over the period 1995–2011.**

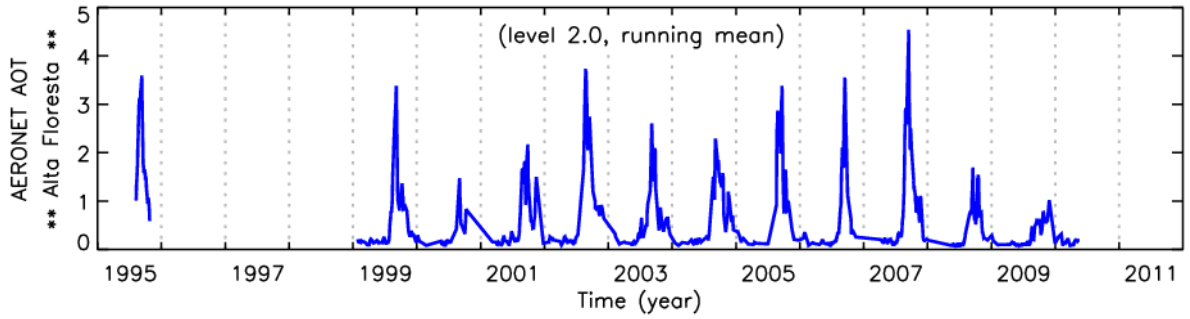

Figure 4: **Aerosol Optical Thickness for AERONET station "Alta Floresta". A running mean of 11 days was applied.**

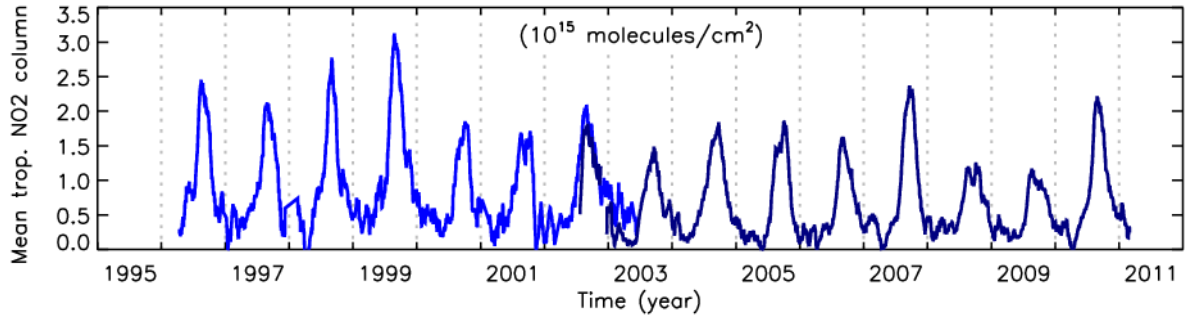

Figure 5: **Mean tropospheric NO_2 column for the Amazonian box as a function of time over the period 1995–2011.**

The correlation between the AAI time series in Figure 3 and the tropospheric NO_2 column in Figure 5 is quite good, even on a quantitative level. This indicates that the seasonal variations in the aerosol presence are well captured by the AAI, but it also yields confidence in the year-to-year variations.

Case C: The Sahel

The aerosol presence in the Sahel region is known to be driven by biomass burning events and/or dust storms, depending on the time of the year. The time series of the regional mean AAI is given in Figure 6. The aerosol presence has a peak in the period between December and March. Looking at the time series of the tropospheric NO_2 column presented in Figure 7, we conclude that this period is dominated by biomass burning. The agreement between the AAI and the tropospheric NO_2 column is again good. The time series of the AAI again shows a stable baseline, supporting the idea that no remnants of instrument degradation have influenced the time series.

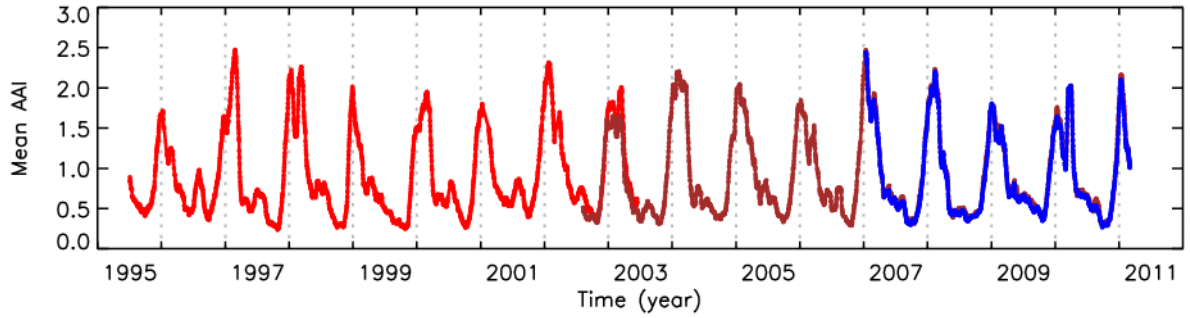

Figure 6: **Mean AAI for the Sahel region as a function of time over the period 1995–2011.**

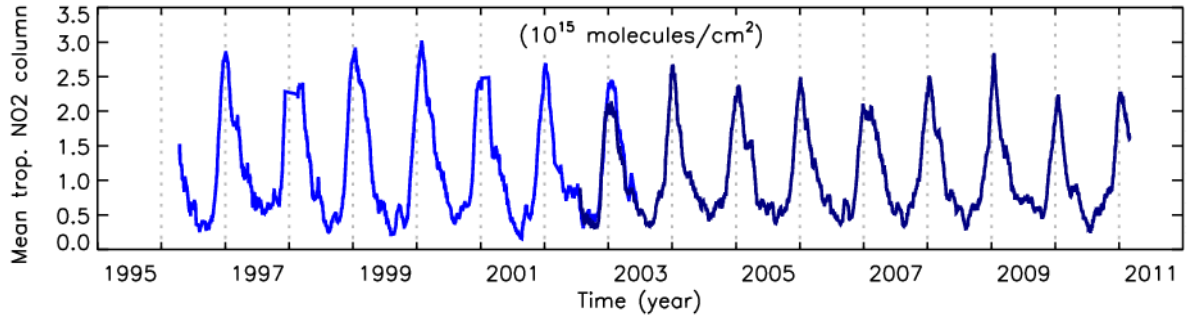

Figure 7: **Mean tropospheric NO_2 column for the Sahel region as a function of time over the period 1995–2011.**

The time series of the three instruments again overlap nicely in the overlap regions. A clear trend in the time series of the regional mean AAI cannot be found.

Case D: West Africa

The aerosol presence in West Africa is well known to be dominated by biomass burning events for most of the year. The time series of the regional mean AAI is presented in Figure 8. The seasonal variation is quite strong, showing a maximum in the period between July and September, and a secondary local maximum in the month of January. This secondary maximum is presumably related to transport of desert dust from the Sahel region. The year-to-year variation in Figure 8 is quite modest.

The time series of the mean tropospheric NO_2 column for the same region is shown in Figure 9. The correlation between this time series and the one presented in Figure 8 is very high. The shapes of the seasonal variation are quite similar. The only difference is that the secondary maxima in the AAI time series do not exist in the NO_2 time series. This would support the idea that the secondary maxima in the AAI time series are indeed not related to biomass burning aerosols, but to desert dust aerosols.

Next, in Figure 10, we present the scatter plot of the regional mean residue versus the regional mean tropospheric NO_2 column. The correlation is surprisingly good, which we attribute to the averaging over space and time. The averaging over space and time is needed to compensate for the different atmospheric trajectories followed by the aerosols and the NO_2 molecules. We conclude that the seasonal variation of the AAI time series is very similar to the seasonal variation of the time series of the tropospheric NO_2 column. Next to this, the year-to-year variation of the AAI seems to be correct.

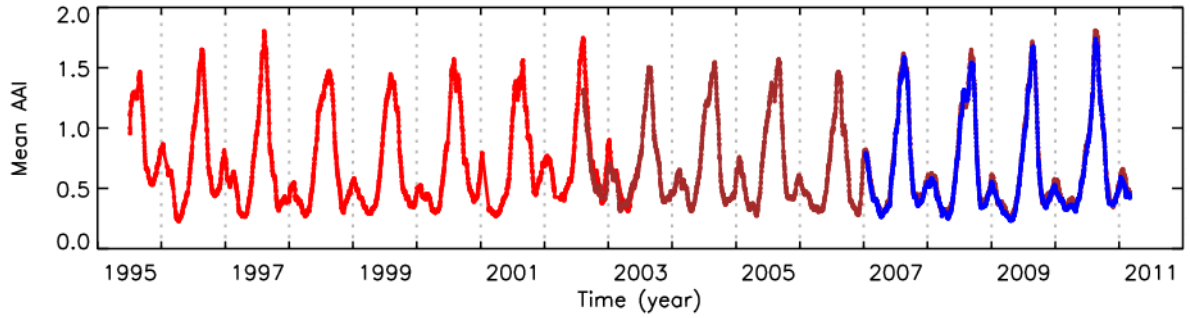

Figure 8: **Mean AAI for the box near West Africa as a function of time over the period 1995–2011.**

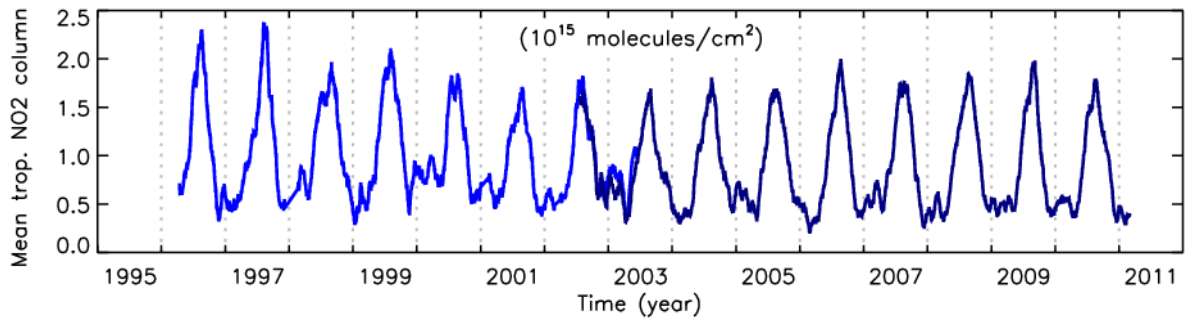

Figure 9: **Mean tropospheric NO_2 column for the box near West Africa as a function of time over the period 1995–2011.**

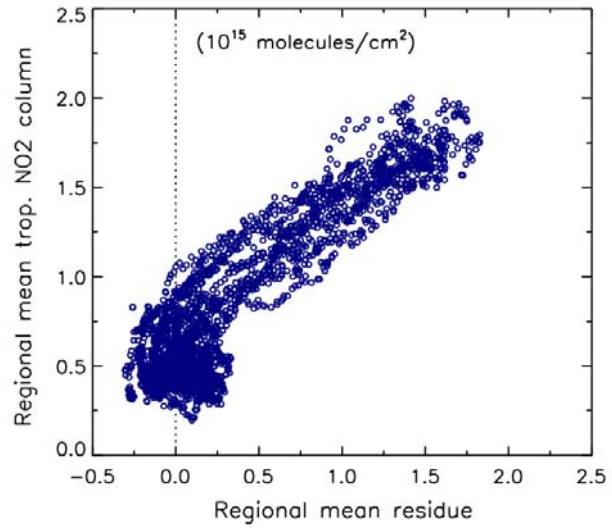

Figure 10: **Regional mean tropospheric NO_2 column versus the regional mean residue for the box near West Africa. There is a clear correlation, at least in the residue regime where aerosols are expected to have been present.**

SUMMARY AND CONCLUSIONS

In this paper we showed that it is possible to successfully combine Absorbing Aerosol Index (AAI) data from GOME-1, SCIAMACHY, and GOME-2 into a 16-year long data archive of aerosol presence. To be able to achieve this, instrument degradation must be accurately corrected for. Using the AAI data, we studied time series of aerosol presence for four typical aerosol regions. The time series showed no

apparent trend, indicating the correctness of the applied correction for instrument degradation. In the overlap periods of the different satellite instruments there was good agreement. The time series were compared with, amongst other things, time series of tropospheric NO_2 data. For scenes controlled by biomass burning events, the agreement was quite good. From this we conclude that we are indeed able to correct for instrument degradation in a sufficient manner. This allows accurate long-term studies of aerosol presence using the AAI. We also anticipate that the combination of the tropospheric NO_2 column with the AAI can be used to verify chemical-transport-models, along the same lines as was done by Veefkind et al. (2011).

ACKNOWLEDGEMENTS

The work presented in this paper was financed by EUMETSAT via the O3M SAF, and by the Netherlands Space Office (NSO) through the SCIA-Visie project. We acknowledge the use of AERONET data and thank Brent Holben for his effort in establishing and maintaining the Alta Floresta site. We also acknowledge the free use of tropospheric NO_2 column data from the GOME and SCIAMACHY sensors from www.temis.nl.

REFERENCES

Tilstra, L.G., Tuinder, O.N.E., Stammes, P., (2010) GOME-2 Absorbing Aerosol Index: Statistical analysis, comparison to GOME-1 and impact of instrument degradation. Proceedings of the 2010 EUMETSAT Meteorological Satellite Conference, EUMETSAT **P.57**, ISBN 978-92-9110-089-7

Tilstra, L.G., De Graaf, M., Aben, I., Stammes, P., (2011) In-flight degradation correction of SCIAMACHY UV reflectances and Absorbing Aerosol Index. J. Geophys. Res., submitted

van der A, R.J., Peters, D.H.M.U., Eskes, H., Boersma, K.F., van Roozendael, M., De Smedt, I., and Kelder, H.M., (2006) Detection of the trend and seasonal variation in tropospheric NO2 over China, J. Geophys. Res., **111**, D12317, doi:10.1029/2005JD006594

van der A, R.J., Eskes, H.J., Boersma, K.F., van Noije, T.P.C., van Roozendael, M. De Smedt, I. Peters, D.H.M.U., and Meijer, E.W., (2008) Trends, seasonal variability and dominant NOx source derived from a ten year record of NO2 measured from space, J. Geophys. Res., **113**, D04302, doi:10.1029/2007JD009021

van der Werf, G.R., Randerson, J.T., Giglio, L., Collatz, G.J., Mu, M., Kasibhatla, P.S., Morton, D.C., DeFries, R.S., Jin, Y., and van Leeuwen, T.T., (2010) Global fire emissions and the contribution of deforestation, savanna, forest, agricultural, and peat fires (1997–2009), Atmos. Chem. Phys., **10**, pp 11707–11735, doi:10.5194/acp-10-11707-2010

Veefkind, J.P., Boersma, K.F., Wang, J., Kurosu, T.P., Krotkov, N., Chance, K., and Levelt, P.F., (2011) Global satellite analysis of the relation between aerosols and short-lived trace gases, Atmos. Chem. Phys., **11**, 1255–1267, doi:10.5194/acp-11-1255-2011

Wooster, M.J., and Strub, N., (2002), Study of the 1997 Borneo fires: Quantitative analysis using global area coverage (GAC) satellite data, Global Biogeochem. Cycles, **16**, 1, 1009, doi:10.1029/2000GB001357